Metallophysics and Advanced Technologies
Металофіз. новітні технол.
Metallofiz. Noveishie Tekhnol.
2024, vol. 46, No. 11, pp. 1051–1065
https://doi.org/10.15407/mfint.46.11.1051
Reprints available directly from the publisher

PACS numbers: 75.50.Bb, 75.50.Tt, 81.05.Ni, 81.07.Wx, 81.20.Ev, 84.32.Hh, 85.70.-w

New Powdered Nanocrystalline Soft Magnetic Composites with Portland Cement Binder

B. S. Baitaliuk, A. V. Nosenko, V. K. Nosenko, and G. A. Bagliuk*

G. V. Kurdyumov Institute for Metal Physics, N.A.S. of Ukraine,
36 Academician Vernadsky Blvd.,
UA-03142 Kyiv, Ukraine
**I. M. Frantsevich Institute for Problems in Materials Science, N.A.S. of Ukraine,*
3 Omeljan Pritsak Str.,
UA-03142 Kyiv, Ukraine

Toroidal cores based on nanocrystalline powder $Fe_{73}Si_{16}B_7Cu_1Nb_3$ (of Finemet type) and Portland cement 'M-500' as a binder are fabricated using powder metallurgy methods (where no pressing is applied). The cores exhibit reliable strength, temperature resistance up to 300°C, and excellent magnetic properties. Using these composites provides lower losses and more stable frequency characteristics of the cores as compared to the cores for power electronics based on carbonyl-iron powders, AlSiFe, or high-silicon electrical steel. Additionally, such composites can be used for production of the devices operating at elevated temperatures, *e.g.*, magnetic flux concentrators for induction heaters. Since these soft magnetic composites do not require pressing operations, the cores' manufacturing process is simplified significantly and enables diversification of core shapes and sizes.

Key words: nanocrystalline alloy, Portland cement, soft magnetic composites, powder cores.

Методами порошкової металургії (без операції пресування) було одержано тороїдні осердя на основі порошків нанокристалічного металевого стопу ММ-11Н складу $Fe_{73}Si_{16}B_7Cu_1Nb_3$ зі зв'язкою на основі портландцементу «М-500». Такі осердя мають достатню міцність, температуростійкість до 300°C, а також відмінні магнетні властивості. Ці композити можуть замі-

Corresponding author: Bohdan Serhiyovych Baitaliuk
E-mail: baytalyuk@ukr.net

Citation: B. S. Baitaliuk, A. V. Nosenko, V. K. Nosenko, and G. A. Bagliuk, New Powdered Nanocrystalline Soft Magnetic Composites with Portland Cement Binder, *Metallofiz. Noveishie Tekhnol.*, **46**, No. 11: 1051–1065 (2024). DOI: 10.15407/mfint.46.11.1051

нити осердя для силової електроніки на основі порошків карбонільного заліза, альсиферу чи електротехнічної висококремністої криці, оскільки мають нижчі втрати та стабільніші частотні характеристики. Також такі композити можуть знаходити застосування у приладах із підвищеними температурами експлуатації, наприклад в концентраторах магнетного потоку індукційних нагрівачів. А оскільки такі магнетом'які композити не потребують операції пресування, то це значно спрощує процес виробництва їх та розширює асортимент форм і розмірів таких композитів.

Ключові слова: нанокристалічний стоп, портландцемент, магнетом'які композити, порошкові осердя, магнетодіелектрики.

(Received 9 July, 2024; in final version, 20 July, 2024)

1. INTRODUCTION

Powder magnetodielectrics have been used in power electronics for quite a long time [1–3]. The cores based on carbonyl iron have been gradually replaced by composite materials based on various alloys. Among them the alloys AlSiFe, AlFe, permendur, Sendust, FluxSan, Permalloy, and others [4–9] are most widely used.

Recently, a new group of soft magnetic magnetodielectrics based on the powders of amorphous and nanocrystalline alloys emerged [10–15]; they are proposed as alternatives to expensive Permalloy cores and demonstrate a wide range of properties that can be tailored to specific applications [16–22]. The combination of high saturation induction, controllable permeability, stable frequency dependence, low core losses, and temperature stability allows for reducing the weight and size of magnetic components used, for instance, in pulse power supplies or telecommunication equipment. Moreover, these new magnetodielectrics are manufactured using substandard waste of amorphous ribbons, which consist mostly of iron and silicon. All of these factors have contributed to the growing use of this new class of composites in the magnetic cores of medium-frequency (from 10 to 200 kHz) transformers, chokes (inductors), converters, and other power electronics applications [23–26].

The main challenge in obtaining such materials lies in the powder compaction operation followed by heat treatment. Amorphous or nanocrystalline powders themselves have high yield strength (and consequently, high hardness), making them difficult to compact [27–29]. To achieve cores with the maximum magnetic filling factor (MFF), it is necessary to apply high pressures (1 GPa and above) [30–32], which significantly complicates the manufacturing technology and increases costs.

Another issue with magnetodielectrics is the low temperature stability of organic binders commonly used to isolate powder particles from each other (to reduce eddy current losses) and to provide sufficient

strength of the composites [33, 34]. Typically, the operating temperature of such composites does not exceed 100–120°C, adversely affecting their magnetic properties and losses. Organic substances like epoxy and phenolic resins, epoxy and silicone-organic varnishes, as well as certain inorganic binders (*e.g.*, silicate glass, TiO_2, SiO_2, ZrO_2, Al_2O_3, NiZr), are frequently used as binders and insulators [35–42]. However, the issue of pressing at high pressures remains, which significantly complicates the manufacturing process.

The choice of binder type represents a compromise between strength, electrical insulation properties, and temperature resistance [43, 44].

2. EXPERIMENTAL PROCEDURE

2.1. Materials

To manufacture the cores, we used a powder of the commercial MM-11H alloy $Fe_{73}Si_{16}B_7Cu_1Nb_3$, which had an amorphous-nanocrystalline structure. As a binding agent, Portland cement of grade 'CEM I' was utilized [45], chosen for its minimal admixture content.

2.2. Preparation of Nanocrystalline Powders

Nanocrystalline powder was obtained by mechanically milling of amorphous ribbon of MM-11H alloy previously annealed at $T_a = 550$°C. The milling process took place in a ball mill for 1 hour in an alcohol environment. After grinding, the powders were dried and separated into fractions.

2.3. Preparation of Soft Magnetic Composites

The manufacturing of the composite cores was carried out as follows.

Nanocrystalline powder was mixed with Portland cement in the following proportions: 80 g of nanocrystalline powder were mixed with 20 g of cement.

Then, water was added to the mixture in an amount no less than required for the complete reaction within the cement. For this grade of cement, it was 25–50% of the cement mass.

The resulting mixture was mixed again until a homogeneous mass was obtained. The mixture was poured into silicone moulds and left to harden at room temperature in the open air.

After 24 hours, the samples were easily removed from the silicone moulds.

The obtained cores had the dimensions as specified in Table 1. Figure 1 shows the photos of the samples before coating (*a*) and after coat-

TABLE 1. Composition, MFF, and physical dimensions of magnetodielectrics with cement binder. MFF is the ferromagnetic filling factor characterizes the volumetric content of the ferromagnetic component in the composite and is calculated as the ratio of the volume of the ferromagnetic component to the total volume of the sample [46].

Core No.	Base composition	MFF	Dimensions $OD \times ID \times H$, mm	S_e, cm^2	l_e, cm	m, g	ρ, g/cm^3
B1	MM-11H + + 20% wt. CEM I	0.33	32×18.5×12.5	0.278	7.93	20.3	3.03
B2	MM-11H + + 20% wt. CEM I	0.31	32×18.5×12.5	0.263	7.93	19.2	2.78

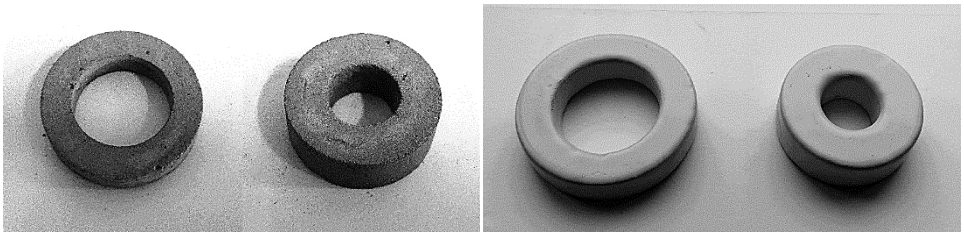

a *b*

Fig. 1. Photos of the cores with cement binder: before coating (*a*), after coating (*b*).

ing with paint (*b*).

2.4. Measuring Magnetic Properties

For powder cores, the dimensions are specified as shown in Fig. 2.

For toroidal powder cores, the effective area S_e is the same as the cross-sectional area times filling factor:

$$S_e = V_e / l_e = m_e \rho / l_e, \quad (1)$$

where m_e is the weight of the ferromagnetic particles, ρ is the density of the ferromagnetic particles.

Ampere's law is correctly written as the integral of the magnetic field H along a closed path l_e:

$$\oint H dl_e = NI, \quad (2)$$

where H is the magnetic field strength vector, dl_e is an infinitesimal vector element of the closed loop, I is current passing through the

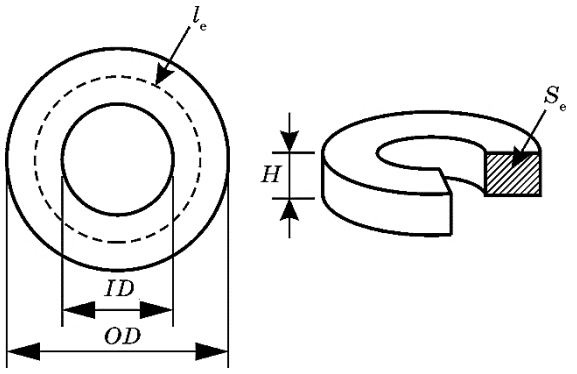

Fig. 2. Schematic image of powder cores.

path, N is number of turns in a coil of wire.

By definition and Ampere's law, the effective magnetic path length is the ratio of ampere-turns NI to the average magnetizing force across the core area, measured from the inside diameter to the outside diameter. Utilizing Ampere's law and averaging the magnetizing force, we obtain the formula for the effective path length. With reasonable accuracy, it is equal to the midline of the toroid, which is defined as:

$$l_e = \frac{\pi(ID + OD)}{2}, \tag{3}$$

where ID and OD are the inner and outer diameters of the toroid, respectively.

The magnetic properties of magnetodielectrics in a constant magnetic field were determined using the Measurement and Information System V5045, designed for the measurement of static magnetic characteristics of soft magnetic materials with coercivity up to 800 A/m under the commutation mode of magnetization on ring-shaped samples, in accordance with the requirements of ДСТУ 8.377-80.

To determine the magnetic characteristics of soft magnetic magnetodielectrics in alternating magnetic fields, the measurement complex for testing toroidal magnetic cores 'MS-02 B-H Analyzer' [47] was used. The inductance of the toroidal cores was determined using the HAMEG LCR Bridge HM8118 measurement complex ($f = 1$ kHz, $U = 1$ V).

2.5. Comparison of the Investigated Composites with Similar Industrial Ones

For an objective assessment of the magnetic properties, the new composite cores were compared with several industrial cores of well-known

TABLE 2. Dimensions and properties of industrial magnetodielectrics [48].There [1] is Fe–Si–Al alloy, [2] is nickel–molybdenum Permalloy, [3] is iron–nickel Permalloy, [4] is Fe–6.5% wt. Si alloy.

Core No.	Brand and marking	Base composition	Density, g/cm^3	Dimensions $OD\times ID\times H$, mm	S_e, cm^2	l_e, cm	μ
C1	Micrometals MS-106026-2	Sendust[1]	5.57	27×15×11.2	0.654	6.35	26
C2	Micrometals MP-106026-2	MPP[2]	6.63				
C3	Micrometals HF-106026-2	Hi-Flux™ [3]	6.65				
C4	Micrometals FS-106026-2	FluxSan™ [4]	6.29				

TABLE 3. Particle size distribution of the powder of the nanocrystalline alloy.

Particle size, mm	Amount, %	Particle size, mm	Amount, %
1–2	0.4	0.16–0.2	13.2
0.63–1	0.7	0.1–0.16	21.6
0.4–0.63	2.5	0.063–0.1	22.7
0.315–0.4	3.7	0.05–0.063	11.0
0.2–0.315	13.5	< 0.05	10.7

brands (Table 2).

3. RESULTS AND DISCUSSION

3.1. Powder Properties

The particle size distribution of obtaining powder is shown in Table 3.

Approximately 90% of the powder has a size of less than 315 μm, indicating a high ability of the annealed ribbon to be milled (see Table 3). Scanning electron microscopy (РЕМ-106И) was applied to analyse the shape and surface morphology of individual particles (see Fig. 3).

SEM showed that the powder is polydisperse, and the particles have a typical shard-like shape with sizes ranging from 1 to several hundred micrometres. The phase composition and nanocrystal sizes of the powder were practically unchanged compared to those of the annealed ribbon of this alloy. Detailed investigations of the crystallization kinetics were conducted in previous studies [49–51].

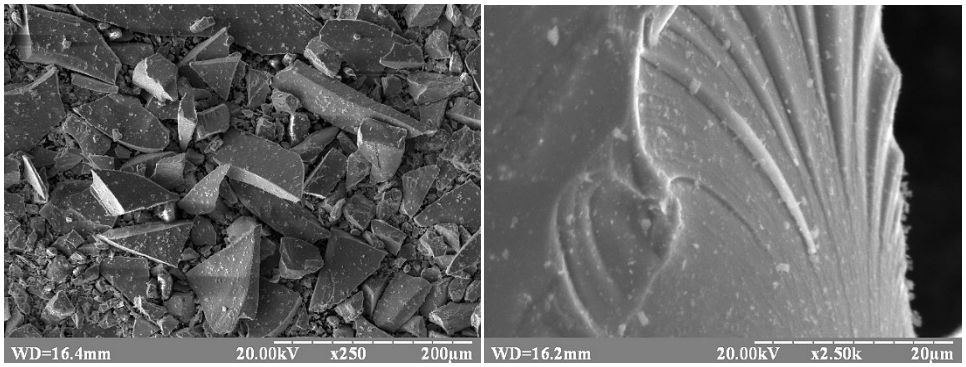

Fig. 3. SEM images of the MM-11H powder after milling: mixture of fractions (*a*), fracture surface (*b*).

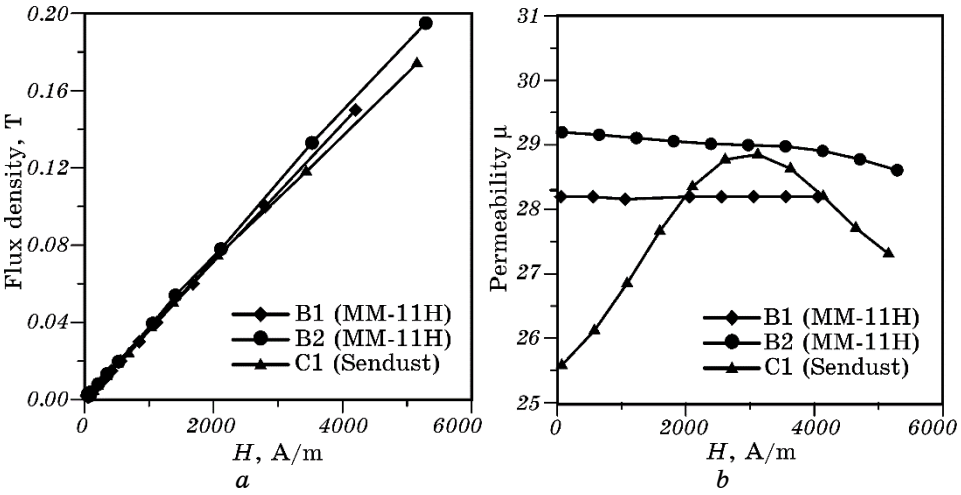

Fig. 4. Segments of the main magnetization curves (*a*) and relative magnetic permeability (*b*) of the samples measured in a DC magnetic field.

3.2. Magnetic Properties of Cement-Binded Composites in DC Field

Figure 4 shows in magnetic properties of the samples in direct current (DC) magnetic field measured in the range from 0 to 5300 A/m.

As can be seen in Fig. 4 the samples with cement binder (B1, B2) have similar relative magnetic permeability in DC field and the same magnetization curve compared to the industrial sample based on Sendust (C1). As one could expect, at so low permeability the magnetization curves are highly linear for both industrial and our samples;

moreover, the samples demonstrated high stability of magnetic permeability in the entire range of magnetic field under investigation.

3.3. Magnetic Properties of Cement-Binded Composites in AC Field

More significant results were obtained when measuring magnetic properties in alternating current (AC) fields (up to 10 kHz) (Table 4).

The difference in the obtained values of the inductance factor A_L (formula (4)) for the 'cement' cores as compared to industrial ones with nearly identical magnetic permeability values is clearly seen when one considers the inductance formula for toroidal cores:

$$L = N_2 \frac{\mu_0 \mu S_e}{l_e} \Rightarrow A_L = \frac{L}{N_2} = \frac{\mu_0 \mu S_e}{l_e}, \quad (4)$$

where N_2 is the number of winding turns, μ_0 is the magnetic constant ($\mu_0 = 4\pi \cdot 10^{-7}$ N/m), μ is the material permeability.

The formula (4) implies that, for the same values of effective magnetic permeability μ the value A_L will be larger at higher values of effective cross-sectional area S_e and smaller values of the average centreline length l_e, and vice versa.

The values of core losses for nanocrystalline cores with cement binder compared to industrial samples are shown in Fig. 5.

As can be seen from Figure 5, the nanocrystalline cores with a cement binder have significantly lower core losses compared to industrial magnetodielectrics. Considering the slope of the logarithmic lines at the frequency 10 kHz, one can see that in the range, where the operating induction exceeds 1000 G, the new nanocrystalline cores with a cement binder surpass all the studied industrial cores in terms of core losses. It can be concluded that all other industrial cores, including those with Mo-permalloy, have higher losses by 30–50% at the operat-

TABLE 4. Magnetic properties of magnetic cores in alternating fields. Core losses at 10 kHz, 0.1 T.

Core No.	Base composition	S_e, mm^2	V_e, mm^3	l_e, mm	μ	P, mW/cm^3	A_L, nN
B1	MM-11N	0.279	7.93	2.21	28	67.6	12.4
B2	MM-11N	0.263	7.93	2.09	29	64.7	12.1
C1	Sendust	0.654	6.35	4.15	26	96	36.4
C2	MPP				24	103.9	32.3
C3	HiFlux™				25	119.7	34.3
C4	FluxSan™				25	175.5	33.8

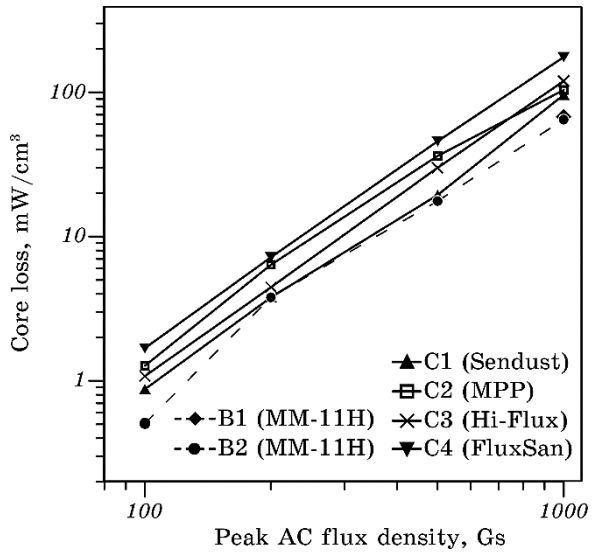

Fig. 5. Core losses in cores at a frequency of 10 kHz.

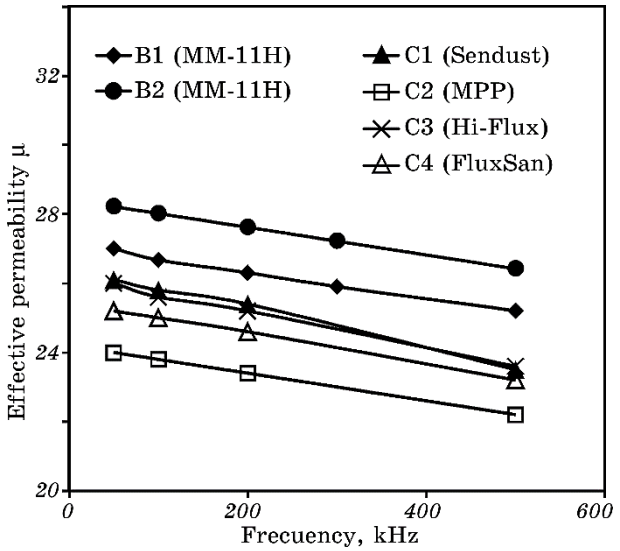

Fig. 6. Core losses in cores at a frequency of 10 kHz.

ing induction of 0.1 T (1000 Gs).

It should be noted that higher values of operating induction are not achieved due to the limitations of the available power amplifier.

The values of effective magnetic permeability vary with frequency as shown in Fig. 6.

In Figure 6, it can be seen that the decrease in magnetic permeability for 'cement' cores in the frequency range of 50–500 kHz is only about 6%, similar to the other industrial cores that were studied.

3.4. Temperature Dependence and Thermal Stability of Cement-Binded Composites

When comparing the change in effective magnetic permeability with the annealing temperature, it is evident that the nanocrystalline cores with cement binding exhibit better temperature stability as compared to the industrial cores (Fig. 7).

Therefore, the effective magnetic permeability of the cores with cement binder increases with annealing temperature (Fig. 7), and at 500°C, this increase is 5% and 9% as compared to the magnetic permeability values of the B1 and B2 samples in the unannealed state, correspondingly. On the contrary, the permeability of all the investigated industrial cores changes significantly already at 300°C, it increased by approximately 20%. This is probably due to the fact that during the manufacturing of the industrial cores, the pressing causes internal stresses, and these stresses are partially relieved during the annealing process. In contrast, the new nanocrystalline cores with cement binder do not experience such stresses because the pressing operation is absent. This explains the small change in their permeability with anneal-

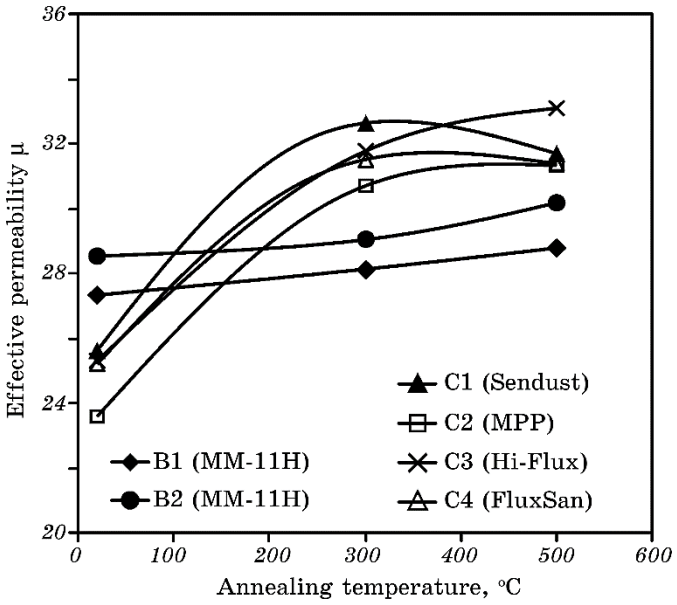

Fig. 7. Core losses in cores at a frequency of 10 kHz.

ing temperature.

We also investigated the temperature dependence of the relative magnetic permeability in the temperature range from 30 to 300°C. The cores with a multi-turn (78 turns) winding of wire with the diameter $D = 0.5$ mm was heated at the rate of 5 K/min, their inductance was continuously measured (with the 10°C step). Permeability was calculated according to the formula (1). The temperature dependence $\Delta\mu/\mu_{20}$ is shown in Fig. 8, *a* (μ_{20} is the effective magnetic permeability at room temperature). From these data, it is possible to analyse the stability of effective magnetic permeability and the appropriate temperature ranges for using the nanocrystalline powder cores with the cement binder.

From the curves shown in Fig. 8, *a*, we can conclude that the maximum thermal stability of the new composite cores is in the temperature range from 20 to 200°C. Starting with 200°C, the magnetic permeability begins to slightly decrease, probably, due to thermal stresses in the composite. However, temperature very weakly affects the magnetic permeability of the cores, and even at 300°C, it decreases only by 3.5%.

Comparing the temperature dependences of magnetic permeability of our and industrial magnetodielectrics, the advantage of nanocrystalline cores with a cement binder becomes evident (Fig. 8, *b*).

In the temperature range 20–160°C, the 'cement' cores demonstrate the best temperature stability. To determine how the magnetic permeability and core losses change in powder cores after the exposure to elevated temperatures, we conducted sequential heat treatments (HT)

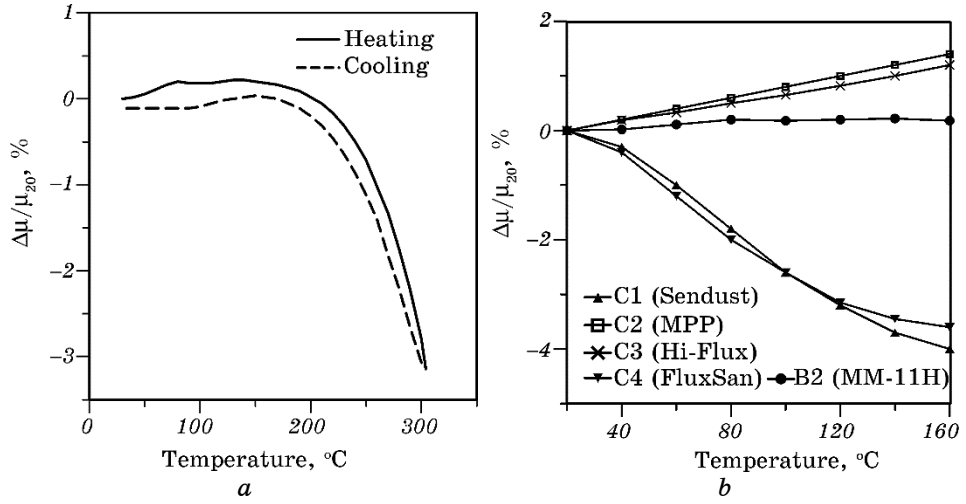

Fig. 8. Dependence of $\Delta\mu/\mu_{20}$ on temperature for nanocrystalline cores with cement binder during continuous heating at a rate of 5 K/min (*a*), temperature dependence of effective magnetic permeability $\Delta\mu/\mu_{20}$ of powder cores (*b*).

TABLE 5. Core losses of powder cores band after annealing.

Core No.	Core losses, mW/cm^3 (10 kHz, 0.1 T)		
	Before heat treatment	Heat treatment 300°C	Heat treatment 500°C
B1	67.6	61.0	65.0
B2	64.7	61.4	62.7
C1	96.0	84.5	90.2
C2	103.9	83.4	87.6
C3	119.7	114.2	126.1
C4	175.5	176.8	171.5

for all cores at 300°C and 500°C; the duration of heating was 30 minutes at each temperature. After each HT, the cores were cooled down, and their properties were measured. The magnetic characteristics of the samples after HTs are presented in Table 5 and Fig. 7.

From Table 5, it can be seen that in all samples there is a slight change in core losses after heating to 300°C (and subsequent cooling). For nanocrystalline cores with cement binding, there is a slight decrease in losses. Even after heating to 500°C for 30 minutes in the open air, nanocrystalline cores with cement binding retain their magnetic properties and strength, which is approximately equivalent to the strength of regular concrete.

3.5. Inductance Factor of Soft Magnetic Composites

Another significant advantage of nanocrystalline composites with cementitious binders is their lower density as compared to well-known magnetodielectrics. To make a fair comparison of the masses and inductances of 'cemented' cores B1 and B2 with the industrial ones, we calculated (based on the results obtained above) the values V_e, S_e, l_e, and A_L for the standard core dimensions of 27×15×11.2 mm. Therefore, at the same dimensions as the industrial magnetodielectrics, the cores B1 and B2 would yield the results shown in Table 6.

From Table 6, it can be seen that, for the same standard geometry, the masses of 'cemented' cores will be half as much as those of the known magnetodielectrics. At the same time, their inductances per unit mass (A_L/m_c) will differ on average by only 20–50%. This ensures greater cost-effectiveness of nanocrystalline cores with cement binding.

4. CONCLUSIONS

Using crushed substandard amorphous ribbons of MM-11H alloy, the

TABLE 6. Magnetic properties of magnetic cores in alternating fields. Calculated values based on the experimental data obtained for B1 and B2.

Core No.	Dimensions $OD \times ID \times H$, mm	S_e, mm^2	V_e, mm^3	l_e, mm	m_c, g	A_L, nN	A_L/m_c, nN/g
B1	27×15×11.2	0.23	1.46	6.35	13.43	12.84	0.96
B2		0.22	1.38		12.70	12.53	0.99
C1	27×15×11.2			6.35	23.12	36.40	1.57
C2					27.51	32.30	1.17
C3					27.60	34.30	1.24
C4					26.10	33.80	1.29

nanocrystalline cores with Portland-cement binding were manufactured. These advanced composite magnetic cores have an effective magnetic permeability of 30 units and core losses of 64.7–67.6 mW/cm^3 (at 10 kHz and 0.1 T), which is approximately 30–80% lower than the losses of industrial magnetodielectrics made of nickel-molybdenum permalloy, iron-nickel permalloy, and Fe–6.5% wt.–Si alloy with the permeability of 26 units, measured under the same conditions. Additionally, these new cores exhibit superior thermal stability of magnetic permeability, retaining their properties even after prolonged heating up to 500°C. This allows them to be used in the conditions where polymer or other organic bindings in most known magnetodielectrics could deteriorate, for example, in magnetic flux concentrators of induction furnaces. Another advantage of such cores is their low density: on average, for the same dimensions, they are half as heavy as the cores made from modern industrial magnetodielectrics.

We sincerely thank LLC ‘MELTA’ for their generosity in providing us with the powders for our research and some the equipment for conducting experiments [52].

REFERENCES

1. Y. G. Guo and J. G. Zhu, *Aust. J. Electr. Electron. Eng.*, **3**, Iss. 1: 37 (2006).
2. N. Ahmed and G. J. Atkinson, *Int. Conf. Electrical Machines (ICEM) (Sept. 5–8, 2022, Valencia)*, p. 551.
3. H. Shokrollahi and K. Janghorban, *J. Mater. Process. Technol.*, **189**, Iss. 1–3: 1 (2007).
4. B. S. Baitalyuk, V. A. Maslyuk, S. B. Kotlyar, and Ya. A. Sytnyk, *Powder Metall. Met. Ceram.*, **55**: 496 (2016).
5. L. I. Rabkin, *Vysokochastotnyye Ferromagnetiki* [High-Frequency Ferromagnetics] (Moskva: GIFML: 1960) (in Russian).
6. *Ferrity i Magnitodiehlektriki: Spravochnik* [Ferrites and Magnetodielectrics:

Handbook] (Eds. N. D. Gorbunov and G. A. Matveev) (Moskva: Sovetskoe Radio: 1975) (in Russian).
7. K. H. J. Buschow and F. R. de Boer, *Physics of Magnetism and Magnetic Materials* (New York: Kluwer Academic/Plenum Publishers: 2003).
8. K. J. Sunday and M. L. Taheri, *Metal Powder Report*, **72**, Iss. 6: 425 (2017).
9. A. Inoue and F. Kong, *Encyclopedia Smart Mater.*, **5**: 10 (2022).
10. S. Lu, M. Wang, and Z. Zhao, *J. Non-Cryst. Solids*, **616**: 122440 (2023).
11. F. C. Li, T. Liu, J. Y. Zhang, S. Shuang, Q. Wang, A. D. Wang, J. G. Wang, and Y. Yang, *Mater. Today Adv.*, **4**: 100027 (2019).
12. G. Herzer, *Acta Mater.*, **61**, Iss. 3: 718 (2013).
13. Y. Y. Zheng, Y. G. Wang, and G. T. Xia, *J. Magn. Magn. Mater.*, **396**: 97 (2015).
14. R. Ma and P. Yu, *Mater. Res. Bull.*, **139**: 111256 (2021).
15. Y. Wang, J. Xu, Y. Liu, and Z. Liu, *Mater. Characterization*, **187**: 111830 (2022).
16. P. Gramatyka, R. Nowosielski, and P. Sakiewicz, *J. Achiev. Mater. Manuf. Eng.*, **20**: 115 (2007).
17. K. L. Alvarez, H. A. Baghbaderani, J. M. Martín, N. Burgos, M. Ipatov, Z. Pavlovic, P. McCloskey, A. Masood, and J. Gonzalez, *J. Magn. Magn. Mater.*, **501**: 166457 (2020).
18. D. Azuma, N. Ito, and M. Ohta, *J. Magn. Magn. Mater.*, **501**: 166373 (2020).
19. P. Gramatyka, R. Nowosielski, P. Sakiewicz, and T. Raszka, *J. Achiev. Mater. Manuf. Eng.*, **15**: 27 (2006).
20. Z. Li, Y. Dong, S. Pauly, C. Chang, R. Wei, F. Li, and X.-M. Wang, *J. Alloys Compd.*, **706**: 1 (2017).
21. C. Chang, Y. Dong, M. Liu, H. Guo, Q. Xiao, and Y. Zhang, *J. Alloys Compd.*, **766**: 959 (2018).
22. Y. Zhang, Q. Chi, L. Chang, Y. Dong, P. Cai, Y. Pan, and X. Wang, *J. Magn. Magn. Mater.*, **507**: 166840 (2020).
23. M. E. McHenry, M. A. Willard, and D. E. Laughlin, *Prog. Mater. Sci.*, **44**, Iss. 4: 291 (1999).
24. B. Ziębowicz, D. Szewieczek, and L. A. Dobrzański, *J. Achiev. Mater. Manuf. Eng.*, **20**, Iss. 1–2: 207 (2007).
25. J. M. Silveyra, E. Ferrara, D. L. Huber, and T. C. Monson, *Science*, **362**, No. 6413: eaao0195 (2018).
26. A. Krings, A. Boglietti, A. Cavagnino, and S. Sprague, *IEEE Trans. Ind. Electron.*, **64**, Iss. 3: 2405 (2017).
27. V. A. Maslyuk, B. S. Baitalyuk, and V. K. Nosenko, *Naukovi Notatky. Inzhenerna Mekhanika*, **25**, No. 2: 150 (2009) (in Ukrainian).
28. S. Yang, J. Xu, M. Tian, J. Wang, T. Yang, G. Li, Y. He, M. Zeng, and X. Liu, *Adv. Powder Technol.*, **34**, Iss. 5: 104024 (2023).
29. J. R. Groza, *Nanostructured Materials* (Ed. C. C. Koch) (William Andrew: 2007).
30. H. Sun, C. Wang, J. Wang, M. Yu, and Z. Guo, *J. Magn. Magn. Mater.*, **502**: 166548 (2020).
31. C. Zhang, P. Tao, K. Zhu, Y. Chen, W. Zhang, and Y. Yang, *J. Supercond. Nov. Magn.*, **34**: 2389 (2021).
32. M. Krasnowski and T. Kulik, *J. Alloys Compd.*, **495**, Iss. 2: 382 (2010).
33. G. Zhao, C. Wu, and M. Yan, *J. Alloys Compd.*, **685**: 231 (2016).

34. X. Chen, Y. Zhang, F. Zhao, M. Tang, M. Xiang, J. Huo, M. Gao, Y. Wang, N. Yodoshi, L. Zhang, and J. Wang, *J. Non-Cryst. Solids*, **616**: 122482 (2023).
35. P. Błyskun, M. Kowalczyk, G. Łukaszewicz, G. Cieślak, J. Ferenc, P. Zackiewicz, and A. Kolano-Burian, *Mater. Sci. Eng. B*, **272**: 115357 (2021).
36. R. Zhao, Y. Dong, S. Wu, X. Li, Z. Liu, X. Jia, X. Liu, H. Wu, W. Gao, and A. He, *Adv. Powder Technol.*, **34**, Iss. 3: 103952 (2023).
37. B. Zhou, Y. Dong, L. Liu, L. Chang, F. Bi, and X. Wang, *J. Magn. Magn. Mater.*, **474**: 1 (2019).
38. Y. Peng, Y. Yi, L. Li, H. Ai, X. Wang, and L. Chen, *J. Magn. Magn. Mater.*, **428**: 148 (2017).
39. Y. Peng, Y. Yi, L. Li, J. Yi, J. Nie, and C. Bao, *Mater. Design*, **109**: 390 (2016).
40. S. V. Chong, W. J. Trompetter, J. Leveneur, F. Robinson, B. Leuw, B. Rumsey, and N. J. Long, *Mater. Sci. Eng. B*, **264**: 114928 (2021).
41. K. Li, D. Cheng, H. Yu, and Z. Liu, *J. Magn. Magn. Mater.*, **501**: 166455 (2020).
42. P. Luo, H. Yu, C. Wang, H. Yuan, Z. Liu, Y. Wang, L. Yang, and W. Wu, *Metals*, **13**, Iss. 3: 560 (2023).
43. V. A. Maslyuk, B. S. Baitalyuk, and H. A. Baglyuk, *Abstr. HighMatTech-2011 (Oct. 3–7, 2011, Kyiv)*, p. 24.
44. Y. Meng, Y. Yang, D. Chen, Y. Zhang, C. Chen, H. Li, and Z. Zhang, *J. Mater. Sci. Mater. Electron.*, **35**: 913 (2024).
45. *EN 197-1. Cement. Part 1. Composition, Specifications and Conformity Criteria for Common Cements* (European Committee for Standardization: 2015).
46. B. S. Baitalyuk, V. A. Maslyuk, and V. K. Nosenko, *Powder Metall. Met. Ceram.*, **51**: 289 (2012).
47. A. Nosenko, T. Mika, O. Rudenko, Y. Yarmoshchuk, and V. Nosenko, *Nanoscale Res. Lett.*, **10**: 136 (2015).
48. *Micrometals*.
49. G. Herzer, *IEEE Trans. Magn.*, **26**, Iss. 5: 1397 (1990).
50. *Handbook of Magnetic Materials* (Ed. K. H. J. Buschow) (Netherlands: Elsevier: 1997), vol. **10**.
51. V. K. Nosenko, *Visnyk Natsionalnoi Akademii Nauk Ukrainy*, **4**: 68 (2015) (in Ukrainian).
52. *Melta*, www.melta.com.ua.